Eurographics Workshop on Visual Computing for Biology and Medicine (2023), pp. 1–10
C. Hansen, J. Procter, and R. G. Raidou (Editors)

Interactive visual exploration of region-based sensitivities in fiber tracking

Faizan Siddiqui[1,2], Thomas Höllt[1], and Anna Vilanova[2]

[1]Delft University of Technology, Delft, The Netherlands
[2]Eindhoven University of Technology, Eindhoven, The Netherlands

Abstract

Fiber tracking is a powerful technique that provides valuable insights into the complex white matter structure of the human brain. However, the processing pipeline involves many sources of uncertainty, with one notable factor being the user-defined parameters that significantly influence the resulting outputs. Among these parameters, the definition of seed-points is a crucial aspect in most fiber tracking algorithms. These seed-points are determined through regions of interest (ROI) and serve as the initial points for fiber tract generation. In this work, we present an interactive technique that utilizes seed-point sensitivities to guide the definition of regions of interest (ROI). We examine various scenarios where sensitivity information can enhance the ROI definition process and provide user guidelines and recommended actions for each scenario. Building upon this analysis, we have developed a visualization strategy that enables users to explore seed-point sensitivities effectively and facilitate the definition of optimal ROIs. We present results highlighting the benefits of the proposed visual design in the clinical pipelines.

1. Introduction

Diffusion Weighted Imaging (DWI) is a non-invasive Magnetic Resonance based technique that allows virtual reconstruction of the brain's white matter and provides insight into the structural organization of the brain's anatomical connections [SKM*90]. DWI works by measuring the diffusion of water molecules within a tissue. Tissue structure, e.g., the axons in the brain, restricts the mobility of the water molecules [Bea02]. This causes anisotropic diffusion. Here, the strongest direction of diffusion indicates the direction of the underlying fibrous structure [BML94], which can be reconstructed by tracking the paths along the strongest diffusion direction [MCCV99; PB96], commonly referred to as fiber-tracking [NGH*05]. This process has proven to be helpful for interpreting brain anatomy [Laz10] and has been used by researchers for several brain diseases [FTC*13; HSO*01]. It has also gained traction in clinical practice, like planning brain tumor resection surgery [OYA*22].

Despite the potential of fiber-tracking methods, several downsides limit their widespread use. Most importantly, the acquired data has to go through a complex transformation and visualization pipeline, accumulating uncertainties at each step [SVBK14; SHV21b]. Apart from uncertainties in the modeling and the acquisition stage [BVPtH09; VW21; TMA*09; SHV21a], uncertainties also arise from various user-defined parameters, such as thresholds or seed-region definition, that significantly affect the resulting fibers [BVPtH09; VW21; TMA*09]. In this work, we investigate the uncertainties involved in the seed-region definition, i.e., regions from which the fiber tracking algorithms start [BPP*00; VES16].

In clinical fiber tracking applications, Regions of Interest (ROIs) like the seed region, are defined by users manually to extract a specific bundle, i.e., a coherent set of fibers connecting two specific regions in the brain. In most cases, users take guidance from anatomical imaging in combination with a 2D directional encoded color (DEC) map (see Figure 1a and 1b). A DEC map encodes the main tensor direction by mapping the (x,y,z)-components of the direction to RGB color channels, respectively, weighted by Fractional Anisotopy (FA) [PP99]. Interactive and automated ROI definition

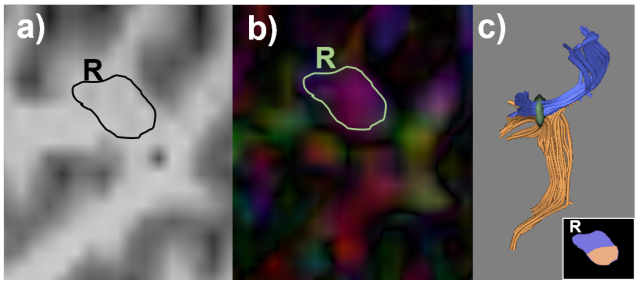

Figure 1: *Potential ROI R overlaid on a T1 image (a) and DEC map (b). In both images, the values in R are homogeneous. However, the resulting fiber tract from the given seed region R is divided into two different fiber bundles (c, orange, and purple) corresponding to a division in the ROI shown in the inset.*

based on the local diffusion properties is well studied [WH11; VW21]. Automatic ROI definition methods often require manual tuning and re-definitions, resulting in a trial and error process, requiring multiple iterations to extract the desired fiber tracts and meet the expectations of the clinician [WH11]. Relying solely on the DEC maps and the anatomical information is sometimes not enough for ROI definition since it only indicates the local directional and anatomical information. Figure 1 shows an example where both the anatomical image (Figure 1a) and the DEC map (Figure 1b) indicate homeogeneouos values within a potential ROI *R*. This could indicate that the fiber tracts seeded from this region may form a coherent bundle. However, the resulting fiber tracts generated from the region R are from two different bundles namely Arcuate Fasciculus (AF) bundle and the superior longitudinal fasciculus (SLF) bundle, as shown in Figure 1c. The resulting fiber demonstrates that there is a division in the region that is not visible on anatomical images and DEC maps, which are the common visualization techniques in a clinical setting.

In this paper, we explore the use of seed-point sensitivity as additional guidance for users. Seed-point sensitivity refers to the variation in fiber tract structures due to slight changes in the seed-point location. By quantifying and visualizing seed-point sensitivity, users can identify the boundaries of desired fiber bundles, aiding in the generation of optimal fiber tracking results. In the example, ROI *R* in Figure 1, such a measure would produce large sensitivity values in the region where the bundle diverges and as such, alleviate the adjustment of *R*. Our main contributions are

- the identification and analysis of scenarios in which seed-point sensitivity can aid in ROI definition,
- corresponding ROI guidance and course of action per scenario for ROI optimization,
- visualization and interaction techniques to guide the definition of ROIs based on the defined scenarios and course of action.

2. Clinical Workflow

To understand the fiber tracking workflow in the neurosurgical setting, we conducted exploratory sessions with our collaborators, which include neurosurgeons, radiologists, and researchers who use fiber tracking for planning tumor resection surgeries. Our clinical collaborators expressed a specific interest in reconstructing the core bundles: Arcuate Fasciculus (AF), Inferior Frontal Occipital Fasciculus (IFOF), Corticospinal Tract (CST), Optic Radiation (OR), and the Frontal Aslant Tract (FAT). These bundles are relevant for neural communication and function in visual perception, recognition, language processing, and motor movements.

Our collaborators employ both automatic and manual pipelines for fiber tracking during preoperative planning. In the manual clinical pipeline, the workflow starts with the image acquisition, followed by the preprocessing of the data, which includes correcting for motion artifacts and eddy currents and normalizing the data to a common space. After the data has been preprocessed, diffusion modeling takes place. The manual clinical pipeline relies on diffusion tensor imaging (DTI) [LMP*01]. However, in our work, other modeling techniques such as HARDI [TRW*02] can also be integrated. After diffusion tensor modeling, ROIs are defined using anatomical information and DEC maps. The ROIs include seed regions and AND regions that are used to filter irrelevant fibers [JLT*13; JC10; MV02; SPW*07]. Using AND ROIs in fiber tracking improves the specificity and reliability of resulting fiber bundles, avoiding spurious fibers. Within the clinical workflow, users manually define ROIs to extract particular bundles. Typically, anatomical cues like T1 images and DEC maps offer partial guidance yet prove insufficient for accurate ROI definition. The task requires multiple iterations to adequately define ROIs, demanding expertise and anatomical insight for optimal accuracy. To circumvent this issue, a guidance strategy is needed to help users in defining desired ROIs. Our collaborators are also testing an automatic pipeline for use in the clinical workflow. Here, ROIs are defined automatically using Spatially Localized Atlas Network Tiles (SLANT) [HXA*18], which use deep learning to compute subject-optimized whole brain segmentations. Fiber tracking is performed using Constrained-Spherical Deconvolution (CSD) method [TCC07]. Although ROIs are defined automatically, manual user input and tuning are needed when the generated results are not adequate.

Our work aims to provide interactive visual guidance in determining ROIs based on seed point sensitivity. Our framework can be used with any diffusion modeling and fiber tracking method that provides fiber tracts through ROI definitions, as we base our sensitivity computation solely on the resulting fiber tracts, i.e., the geometrical features of the fiber tracking results. We demonstrate the feasibility of our framework by utilizing both the manual and automatic workflows of our collaborating partners.

3. Related Work

In this section, we provide a comprehensive review of the literature that is relevant to our work, specifically focusing on studies that investigate fiber tracking parameters and their sensitivities, as well as the definition of ROIs. In addition, we also examine related work on the visual encoding of multiple scalar fields along with the discussion on coherence measures. Our primary emphasis is on papers that explore sensitivities and ROIs.

The fiber-tracking pipeline comprises several input parameters that control the tracking process. The most critical user-defined parameters are Fractional Anisotropy (FA) thresholds and ROIs. Taoka et al. [TMA*09] evaluated the influence of FA thresholds in measuring diffusion tensor parameters for tract-based analysis. Gutierrez et al. [GSN*20] presented a framework to optimize FA thresholds of fiber tracking algorithms using multi-objective optimization techniques. Brecheisen et al. [BVPtH09] evaluated the sensitivity of FA thresholds in fiber-tracking algorithms and provided an interactive visualization for parameter exploration.

Schlaier et al. [SBF*17] studied the influence of seed regions to delineate cerebellar-thalamic fibers in deep-brain stimulation and analyze how seed regions affect the results in both deterministic and probabilistic fiber tracking. Huang et al. [HZVM04] assessed the effects of noise, ROI size, and location on DTI-based fiber reconstruction results for one-ROI (i.e., seed region only) and two-ROI approaches (i.e., seed region plus AND regions). They analyzed the differences in the resulting tracts by dilating the ROI size and perturbing the location. Even though the study was principally focused

on comparing one- and two-ROI approaches, they concluded that the ROI placement could be a major source of poor reproducibility in fiber tracking. Several approaches have been proposed in the literature to automatically define ROIs [HLZ*22; EYQ*20]. Weiler et al. [WH11] employed local diffusion parameters, such as fractional anisotropy and radial diffusivity, to generate automated ROIs for fiber tracking. Despite the existence of automatic methods, manual user input in ROI definition is still needed in complex cases. Schonberg et al. [SPH*06] propose to use functional MRI (fMRI) data to define ROIs for adequate fiber tracking results, especially when ROIs have to be placed within or in the vicinity of a lesion. The presence of lesions deforms the fiber structures, affecting the DEC map and T1 image and thus impeding ROI definition. In complex cases, fMRI data is also affected by edema or glioma. Voltoline et al. [VW21] proposed to combine shape and FA information and show them as glyphs to guide ROI definition. To the best of our knowledge, there has been no research on the inclusion of seed-point and ROI sensitivities.

The use of tensor lines to visualize tensor fields is closely related to vector field visualization using integral curves, modeling the trajectories of particles through the field. Visualizing the coherence of motion among neighboring particles has been studied in this context [CMLZ08; LSM07; SP07; GGTH07]. These approaches locally express the change of the particle trajectory with a variation of the initial position. Hlawitschka et al. [HGT*10] presented an approach based on similar concepts applied to tensor lines. They introduced a coherence measure defined for fiber tracts and provided an effective visualization to represent the fiber coherence combined with the existing visualization. Moberts et al. [MVV05] and Qazi et al. [QRO*09] discuss measures for the quantification of coherence of neighboring fibers in diffusion tensor data. In our work, we use existing coherence measures based on the global geometrical shape to compute the sensitivity of seed point placement and provide guidance to the users to define an optimal ROI. To the best of our knowledge, no related work proposes using sensitivity analysis for ROI definition and guidance in fiber tracking workflow.

Numerous contributions have been presented in the literature concerning the visual encoding of multiple scalar fields, encompassing measures like coherence, hemodynamics, uncertainty, etc. Meuschke et al. [MVB*16] introduced a method for concurrently displaying two scalar fields for the visual analysis of aneurysm data, aiming to enhance insights into complex anatomical structures. The first attribute is color-coded, while the second utilizes an image-based hatching scheme. Building on this foundation, Meuschke et al. [MGB*18] further proposed a checkerboard visualization that facilitates the simultaneous exploration of diverse attributes. Hlawitschka et al. [HGT*10] adopt a continuous scalar map with distinct color scales to represent point-wise coherence measures. In our work, we embrace a similar concept, utilizing an interactive discrete color map for scalar field visualization to mitigate visual clutter and effectively portray sensitivity alongside anatomical information.

4. Sensitivity Analysis

Based on the sensitivity definition [Cac81], we present the seed-point sensitivity as the relation of a slight change, $\delta\mathbf{s}$, in the seed-point position, $\mathbf{s}$, and the amount of change of the resulting fiber tract, $f(\mathbf{s})$, i.e., amount of change of seed point, $||\delta\mathbf{s}||$ versus distance between resulting fiber tracts $d(f(\mathbf{s}+\delta\mathbf{s}), f(\mathbf{s}))$.

We calculate the seed point sensitivity in a predefined grid as a scalar field. To do so, we first assign a sensitivity value S_i to each seed-point position $\mathbf{s}_i$. S_i is defined as the mean of the distances of its corresponding fiber F_i to all other fiber samples within a radius $||\delta\mathbf{s}||$. The sensitivity S_c for each grid cell c in the field is then calculated by averaging the sensitivity values S_i of each seed point within the cell. The resolution of the grid can also be adjusted to achieve the desired precision. Seed points are distributed randomly within the cell based on the predetermined number of fibers per grid cell. However, when pre-computed fibers are utilized, the quantity of fibers per cell depends on the defined fiber density parameter.

There are various options to define the distance $d(f(\mathbf{s}+\delta\mathbf{s}), f(\mathbf{s}))$, depending on the goal. Here, we focus on definitions that consider the geometrical properties of the fiber tracts since the evaluation of the fiber bundle relies primarily on the geometry of the tracts. Other sensitivity parameters, e.g., diffusion properties [HGT*10], could also be incorporated. There has been a considerable amount of research on similarity measures between fiber tracts and, more generally, integral lines or curves in vector field [JPS*10; CFJ*05; Goo09]. The first category measures the Euclidean distance between pairs of points on two curves, such as the closest point measure, the Hausdorff distance [RW09], or the Fréchet distance [AG95]. A second category is the mean Euclidean distance along the run lengths of the curves, such as the mean distance of closest distances [CGG04] or the mean threshold closest distances [ZDL03]. There are also distances computed based on Euclidean space embedding of the curves, such as the Gaussian kernel distance [BKP*04]. Each of these measures has its own strengths and limitations in terms of sensitivity and invariance. In our work, we focus on the coherent geometrical features of fiber tracts as it is considered an essential criterion that characterizes bundles. A general assumption is that the fiber tracts belonging to the same bundle have smoothly changing geometrical properties. We explore distance-based metrics, as discussed by Moberts et al. [MVV05] and Corouge et al. [CFJ*06]. We compute the distance measure d between the fiber tracts F_i and F_j using the mean of the closest point distance, which is proven as a relevant distance measure for automatic clustering for bundle identification [MVV05; CFJ*06]. The distance is defined as:

$$d_m(F_i, F_j) = \underset{\mathbf{p}_i \in F_i}{\text{mean}} \min_{\mathbf{p}_j \in F_j} ||\mathbf{p}_i - \mathbf{p}_j|| \tag{1}$$

where the minimum distance for each point $\mathbf{p}_i$ of F_i to the points $\mathbf{p}_j$ of F_j is computed, and then the mean of all closest distances of $\mathbf{p}_i$ to F_j is used. Notice that d_m is not symmetric; therefore, the distance between the two fiber tracts d is then computed by $\min(d_m(F_i, F_j), d_m(F_j, F_i))$. Using the minimum allows us to account for different fiber lengths. Other distance measures to calculate the similarity between two curves can be integrated into the pipeline. The choice depends on the specific case to be explored and the fiber tracking algorithm used.

5. Scenario Analysis

To support ROI definition in a structured way, we analyze different scenarios in relation to the use of computed sensitivities for ROI definition. As discussed in Section 4, fiber tracts belonging to the same bundle generally have similar or smoothly changing geometrical features. Our assumption is that sensitivity can indicate potential boundaries of bundles that indicate relatively large sensitivity. In the following, we follow previous works [MVV05; JD88; JMF99] and use the terms **complete** and **correct** to evaluate the fiber tracts, resulting from a defined ROI. Here, correctness means that all produced fibers belong to the correct bundle, while completeness means that all fibers belonging to a specific bundle are produced. Given the absence of ground truth in fiber tracking data and our goal being to support the interactive definition of ROIs, correctness, and completeness rely on the specific user requirements and may differ from user to user. Hence, we provide the guidance strategy based on the defined assumptions of similarity and continuity of bundles but ultimately leave it to the user's discretion to decide.

Figure 2 illustrates four basic scenarios concerning sensitivity based only on the seeding ROI. To explain the possible scenarios, we give an example of a region where two different bundles are diverging and close to each other. We are interested in generating one fiber bundle. The area where the bundles meet can also be identified and investigated with the sensitivity map. For simplicity, we only show two sensitivity levels: dark for high sensitivity and light for low sensitivity. The black outline represents the seed ROI, and the blue curves depict fiber tracts. Solid curves show selected tracts, while transparent ones display filtered fibers based on defined ROIs.

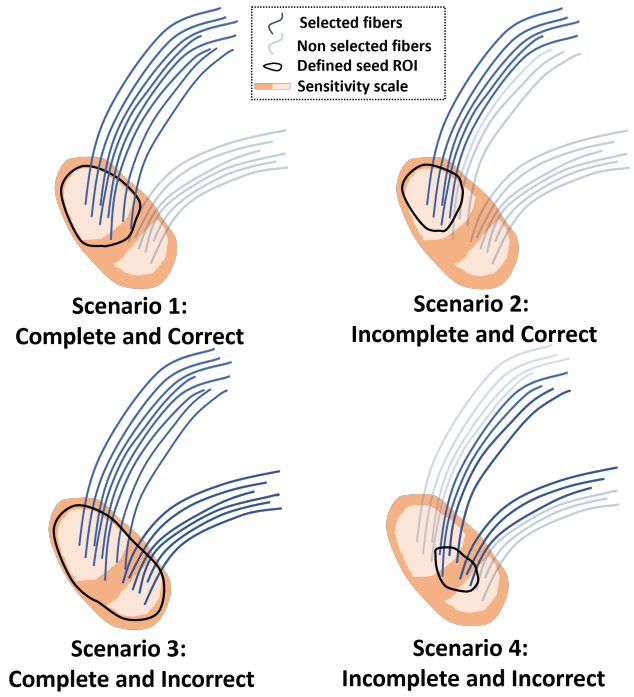

Figure 2: *Illustrations of the possible scenarios for ROI definition.*

Scenario 1 in Figure 2 shows the ideal case where all fibers of the desired bundle are produced, i.e., **complete and correct**. This situation occurs when the ROI extends to the boundary between a low and high-sensitive area without including parts of the high-sensitivity area. **Scenario 2** shows the case where the seed ROI does not produce the whole bundle, i.e., the produced fibers are **correct** but **incomplete**. The defined region needs to be *extended* to cover the complete bundle. In **Scenario 3**, the defined seed ROI has two low sensitivity areas divided by a high sensitivity area depicting that the resulting fibers are **complete**, but due to coverage of an incorrect region, some of the fibers are **incorrect**. The ROI needs to be *shrunk* to only one of the low sensitivity areas. **Scenario 4** shows the combination of Scenarios 2 and 3, where the seed ROI contains low and high sensitivity areas; hence, the resulting set of fibers is **incomplete and incorrect**.

As discussed in Section 2, users employ AND ROIs, in addition to the seed region in most clinical cases, to extract specific fiber bundles [BPP*00]. We extend the previously discussed scenarios by adding an AND region. We do not consider Scenario 4 as it is a local combination of other scenarios. The scenarios summarized in Figure 3 specify the characteristics of the defined ROIs and the corresponding fiber bundle selection. As previously discussed, we distinguish the ROIs in each scenario based on the completeness and correctness of the selected fiber bundle. In Scenario 1.1, both the Seed and AND ROIs generate complete and correct fiber tracts. The combination of these defined ROIs results in a complete and correct fiber bundle. All scenarios with the addition of an AND ROI (represented with the green area) are illustrated in Figure 4. The glyph on the top left shows the scenario according to Figure 3.

In Scenarios 1.x, the seed ROI is defined as complete and correct, as discussed earlier. Therefore, only a too-small AND ROI impact the result, thus producing an incomplete result (Scenario 1.2). Here, the AND region needs to be extended or removed.

In Scenarios 2.x, the seed ROI misses similar fibers which belong to the desired bundle. Therefore all scenarios are incomplete. This cannot be addressed by adjusting the AND ROIs. Thus, the user will want to extend the seed ROI to be complete and correct. The result will be the corresponding Scenarios 1.x.

In Scenarios 3.x, the seed ROI covers fiber tracts from different bundles generating complete but incorrect results. In Scenario 3.1, the AND ROI makes the result complete and correct being the only

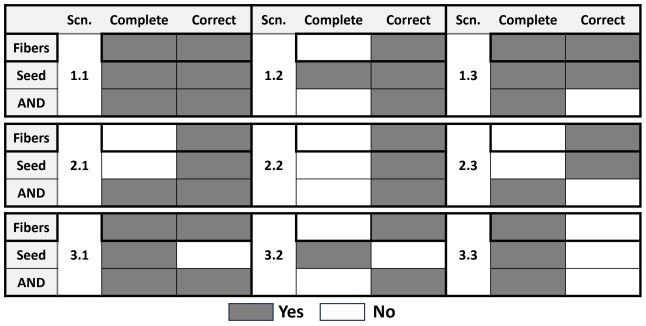

Figure 3: *Summary of the characteristics of the Seed and AND ROIs and their combined effect for each scenario.*

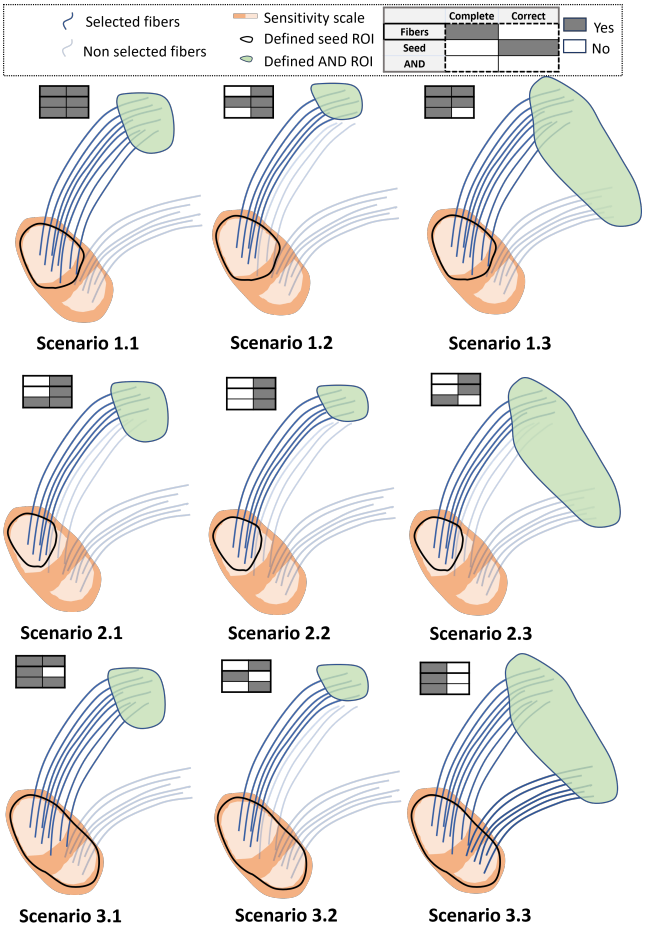

Figure 4: *Illustrations of the possible scenarios for the definition of the seed and the AND ROI. The glyphs at the top left for each scenario refer to the scenarios illustrated in Figure 3.*

scenario in 3.x that generates such an outcome. In Scenario 3.2, the AND ROI is incomplete. In this scenario, a user can shrink the seed ROI to get Scenario 1.2 or extend the AND ROI to get Scenario 3.1. Similarly, in Scenario 3.3, both ROIs generate complete but incorrect results. The user can shrink one of the ROIs to get either Scenario 1.3 or 3.1. A summary of the corresponding courses of action to reach the complete and correct results (i.e., Scenarios 1.1, 1.3, and 3.1) is illustrated in Figure 5.

6. Visualization Design

In this section, we discuss our proposed visualization design to facilitate the interpretation of sensitivities based on the scenarios and corresponding actions to aid the ROI definition described in Section 5. We used anonymized DW-MRI data sets of two different patients provided by our collaborators. The volume data sets comprise of $128 \times 128 \times 60$ voxels, with a resolution of $1.75 \times 1.75 \times 2\text{mm}^3$. The scanner parameters are b-value$= 1{,}000$ and gradient-directions$= 32$.

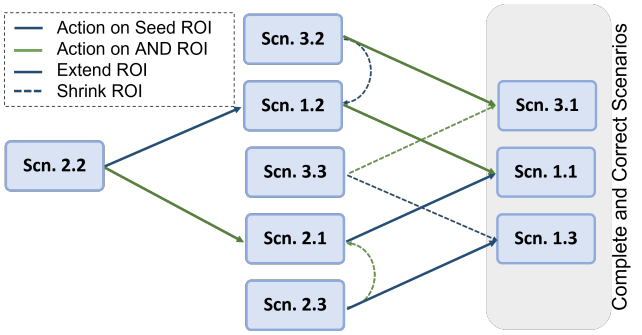

Figure 5: *Action sequences to reach the complete and correct scenarios.*

6.1. Sensitivity Maps

Our aim is to provide sensitivity information, which we derive as a scalar field (Section 4), alongside the DEC map and anatomical information commonly used in clinical settings. This combination serves to provide guidance for ROI definition. Understanding the seed-point sensitivity within and near the ROI is the basis for identifying the course of action (Section 5).

A straightforward approach to visualize the calculated sensitivities is to use quantitative color maps. The maps can be overlaid on top of the anatomical slices or the DEC map. However, the overlaying of the color map occludes structures presented in the DEC

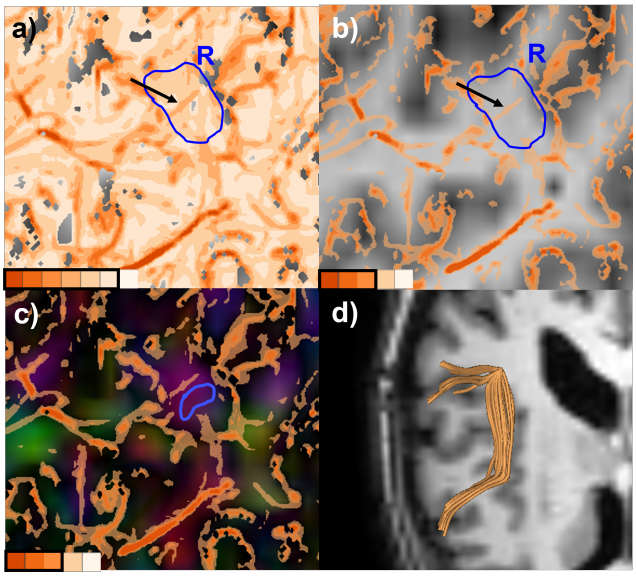

Figure 6: *The sensitivity map is represented as a discrete color map with a) 7, b, c) 5 bins. The number of bins and transparency are adjusted to reduce cluttering. Seed ROI for different cases is represented with the blue curves, and the fiber tracts are rendered as shaded tubes shown on the 3D view in d). The black arrow highlights the high sensitivity area within the region R. The color scale is shown at the bottom left.*

map and the anatomical slice. To circumvent this problem, we propose to use a discrete color map with a limited number of bins (e.g., defined using ColorBrewer [HB03] for sequential data). Based on the proposed interactions and guidance strategy in the previous section, the focus is on identifying and visualizing the highly sensitive regions. Anatomical information, e.g., T1 images, use luminance values to represent the data, while DEC maps use hue channels to encode the tensor directional information. To distinguish our sensitivity map when combined with the anatomical information and the DEC map, we chose a color map that is distinguishable and minimally interferes with the hue of the DEC map. Moreover, we enable users to interactively set and adjust the number of bins to be visualized such that they are more clearly recognizable. Commonly, a relatively low number of bins will be used, making the boundaries of the bundles more obvious. The user can adjust the transparency of each bin, which helps combine different information from the other scalar fields. Figure 6 illustrates the color overlay using the case shown in Figure 1. Figure 6a, Figure 6b, and Figure 6c show the sensitivity map for two different bins, 7 and 5, overlaid on T1 and the DEC map with adjusted transparencies. The sensitivity map is generated with 8x resolution and a neighborhood window of 5x5x5 voxels. We use the Colorbrewer *OrRd* color map, with the higher bins made more opaque while the lower bins are semi-transparent. In this way, only the regions with high sensitivities are highlighted. The color maps are shown at the bottom left insets in Figure 6 with a black border representing non-transparent bins. As can be seen in Figure 6a, a higher number of bins provides more detailed sensitivity distribution but makes the visualization overly complex and cluttered. The number of bins and transparency both are adjusted, as shown in Figure 6b and Figure 6c, making it easier to identify different sensitivity levels with less cluttering on the anatomical information. The same region *R* introduced in Figure 1 is selected as a seed region, which shows a uniform coloring in the DEC map and anatomical slice. Our sensitivity map shows a high-sensitivity region that suggests a boundary cutting the region in two, as shown in Figure 6. The black arrow points to the high sensitivity area within the region *R*, depicting that the ROI contains seeds for two different bundles (Scenario 3) as shown in Figure 1c. As expected, the generated fiber tracts are diverging since the ROI encompasses two individual homogeneous sensitivity regions separated by high sensitive boundaries. The sensitivity map makes it easy for the user to identify the boundary between the two bundles and thus helps in optimizing the ROI. Following the guidance strategies as explained in Section 5, the ROI needs to be shrunk to extract a coherent set of fibers, as shown in Figures 6c and 6d.

It is important to note that the computation of the sensitivity as a scalar field can be computationally expensive, with the computation time dependent on both the neighborhood size and the sampling rate within each fiber. We use the same sampling as the integration step of each fiber. The overall computation time for the sensitivity calculation for each cell is around 0.025 seconds for the neighborhood size of $5 \times 5 \times 5$ voxels. To further accelerate the interactions, we enable progressive computation of the sensitivity map in the background, allowing users to continue exploring sensitivities and defining regions of interest (ROIs) without any delay. The computations start from a user-selected ROI progress throughout the plane until the desired area has been computed. The framework also supports the utilization of precomputed fiber tracts and sensitivity maps for ROI definition.

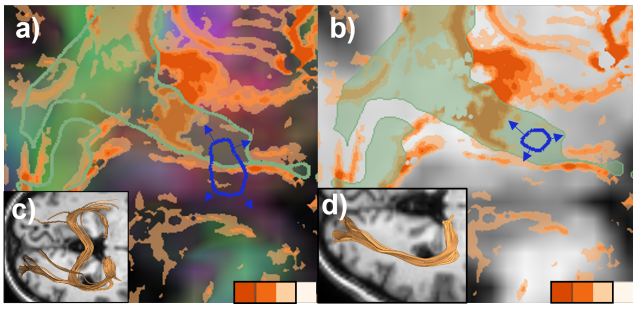

Figure 7: *ROI projection is represented as a green semi-transparent overlay on the top of a) direction-weighted FA map b) T1 slice with overlaid sensitivity map. The defined seed ROI is represented with a blue curve. The corresponding fiber tracts are shown in c) and d), representing the 3D orthogonal views. Guiding glyphs are shown at the boundaries of the defined ROI.*

6.2. AND ROI projection

As discussed in Section 2, AND ROIs are used to filter the fiber tracts. The most relevant information for the user defining the seed ROIs is whether the region being analyzed is connected to the defined AND ROI. We provide this information by a projection of the AND ROI in the seed ROI area. The projection is calculated by marking the voxel if at least one fiber traced from the cell intersects the defined AND ROI. It is worth mentioning that the projections only rely on the slice being analyzed for seeding; hence, there can be areas of the AND ROI that are not projected. The projection is basically a binary mask that we use in combination with the seed ROI sensitivity. The computed projection is represented as a green semi-transparent area overlaid on the top of the sensitivity map and the anatomical slice, representing the complete area where the fiber tracts are connected to the defined AND ROI. We have used a green overlay on the top of *OrRd* color scale of the sensitivity map, combined with an anatomical slice according to the diverging color suggestion from Colorbrewer. Since the DEC map uses hue as a channel to encode the directional information and uses the full range of color tones, there is interference. We outlined the binary map to make the projections more distinguishable and recognizable. We provide interactive means to define and optimize the seed and AND ROIs by simply brushing on the corresponding slices. Derived data, such as the AND region projection, are linked and updated interactively.

Figure 7 illustrates an example of the generation of OR bundle that connects the lateral geniculate nucleus (LGN) to the primary visual cortex and is responsible for transmitting visual information from the retina of the eye to the visual cortex. In most clinical cases, the AND ROIs are also needed to optimize the resulting fiber tracts. Figure 7a shows the initial seed ROI along with the AND ROI projection. The curved course, the sharp turn of the OR, and their proximity to other white matter tracts, including the uncinate fasciculus, the Inferior Fronto-Occipital Fasciculus (IFOF),

and the inferior occipito-temporal fasciculus, make its ROI definition quite challenging. The defined seed ROI is represented with a blue curve, and the corresponding generated fiber tracts are shown in Figure 7c-d. As can be seen in Figure 7a, the defined seed ROI contains a high sensitivity region, corresponding to Scenario 4. The AND ROI in OR is usually fixed as the bundle terminates in the primary visual cortex. Given the projection information and guidance strategy from Scenario 3.3, the user can modify the seed ROI to get the adequate bundle, as shown in Figure 7d. The ROI can be further adjusted per suggestions to achieve the desired bundle.

6.3. Guiding Glyph

In addition to visualization of the sensitivity based on color maps, we provide further guidance based on Scenario 2 (see Section 5), which indicates that the sensitivity just outside the defined ROI is homogeneous. The ROI can be extended, suggesting coherent fiber tracts in the vicinity. We use glyph-based visual cues to convey the sensitivity information outside of the currently defined ROI and guide the user on where to extend the ROIs to encompass the coherent fibers. We use simple arrow-based glyphs placed orthogonal to the boundary of the defined ROI. The direction of the arrow indicates the potential direction of extension based on the sensitivity value at the given point, as shown in Figure 7. The length of the arrow indicates the inverse of the sensitivity at the given position, which means that if the sensitivity value is low, the arrow will be longer and vice-versa. The arrows are only visible when the sensitivity value at the given position is lower than a certain threshold and when there is no need to extend the ROI. This visual cue guides the user to extend the defined ROI until the sensitivity at the boundaries is high, as explained in seed ROI scenarios 2 and 4 in Section 5. As shown in Figure 7b, the defined seed ROI covers the incomplete OR bundle corresponding to Scenario 2 and is guided to extend the ROIs.

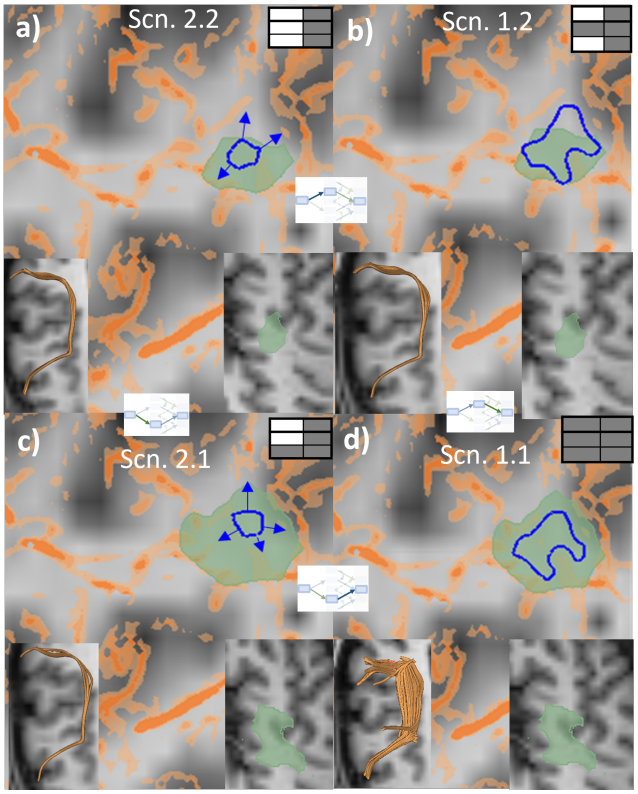

Figure 8: *ROI definition for Arcuate Fasciculus (AF) bundle. The definition starts with incomplete ROIs and is guided till the complete and correct bundle is generated based on the provided guidance. The glyphs refer to the action sequence shown in Figure 5.*

7. Results

In this section, we present use cases of our visualization and initial feedback from our clinical partners with whom we developed the system. We have conducted feedback sessions with two of our collaborators during the course of this work. We explore the definition of ROIs for two fiber tract bundles using two different pipelines and fiber tracking techniques. We analyzed the Arcuate Fasciculus (AF) bundle generated with the manual pipeline using DTI and the Frontal Aslant Tract (FAT) generated with the automatic pipeline using CSD. All computations were performed using an Intel (R) Core i9-9900K CPU (3.6 GHz). Our framework is implemented in C++ and Python as a plug-in for the open-source medical image processing and visualization framework 3D Slicer [FBK*12]. The parameters for the fiber tracking are suggested by our collaborators, which include the stopping FA threshold= 0.2, integration step length=0.5mm, and stopping curvature= 0.7.

In Section 6.1, we explored the computed sensitivity map to adequately define seed ROI for Arcuate Fasciculus (AF) bundle. We start our analysis by defining the ROIs based on anatomical knowledge and utilizing the sensitivity map by interactively selecting the region and visualizing the corresponding fibers, as shown in Figure 6. It is to be noted that the region manipulation and visualization are interactive and are done in real time. As discussed, AND regions are also incorporated by users to filter out undesired fiber tracts during fiber bundle definition. To aid users in this process, our framework introduces a projection visualization of the AND region, which enables them to comprehend the connectivity of fiber tracts. Figure 8 depicts a use case where the user defines the ROIs based on the provided sensitivity visualization and guidance. The definition starts with an initial placement of ROIs, as discussed in Section 6.1. The initial AND ROI, shown at the bottom right, is defined by our collaborators based on anatomical knowledge. The projection of the AND region is shown as a green transparent surface on the top of the sensitivity map, along with the defined seed ROI and the anatomical information. It can be observed that the AND and the seed ROIs do not cover the whole region where the sensitivity is low, indicating that the case is potentially incomplete, corresponding to Scenario 2.2, as shown in Figure 8a. There is a homogeneous low sensitivity region outside of the boundaries. As fiber tracts within a low sensitivity region are assumed to have belonged to the same bundle, some desired tracts are missed in this case. The suggested actions is either to extend the seed ROI to achieve Scenario 1.2 (Figure 8b) and modify the AND region to reach Scenario 1.1 (Figure 8d). The other option is to extend the AND region first,

as shown in Figure 8c, and then extend the seed ROI based on visual cues to achieve the final correct state, as shown in Figure 8d. The inset images between the figures represent the course of action to go from one scenario to another, as explained in Section 5.

In our second case, we employed our developed framework to refine the ROIs of the automated pipeline used by our collaborators. As detailed in Section 2, the automated pipeline employs SLANT for automatic ROI definition and subsequently utilizes the CSD method for fiber tracking. Nevertheless, in certain scenarios, manual adjustment of the automatically generated ROI becomes necessary if the resulting fiber tracts are not adequate, especially in the presence of a tumor. The automatic pipeline is not interactive and requires repeated rerunning after each adjustment of the ROI. Here, we present a case on tuning ROIs for the Frontal Aslant Tract (FAT) bundle. Figure 9 shows the initial ROI represented with a blue curve overlaid on the DEC map and anatomical slice, which shows the homogeneous distribution. The resulting fiber tracts are displayed in the inset figure with coronal and axial views. It is observed by our collaborators that the resulting fiber tracts also encompasses the fibers from the neighboring bundle. We employed our visualization strategy to tune the ROIs aiming to achieve a complete and correct bundle. The sensitivity map is generated using 8x resolution and $5 \times 5 \times 5$ of neighborhood window. Figure 10 shows the computed sensitivity map overlaid on an anatomical T1 slice,

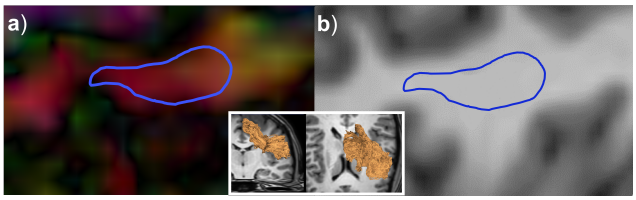

Figure 9: *ROI used by the automatic pipeline, shown with the blue curve, overlaid on the a) DEC map and b) Anatomical slice. The region shows the uniform distribution, Inset: Coronal and Axial views of the resulting fiber tracts.*

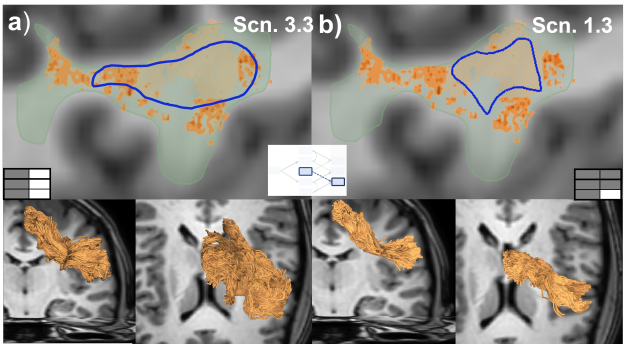

Figure 10: *ROI definition for Frontal Aslant Tract (FAT) bundle using automatic pipeline. The definition starts with incorrect ROIs and is guided till the complete and correct bundle is generated based on the provided guidance. The inset refers to the action sequence shown in Figure 5.*

while the resulting fiber tracts are displayed at the bottom section with coronal and axial views. As shown in Figure 10a, there are regions of high sensitivity within the initial seed ROI, representing the boundaries among distinct bundles. This information is not visible in the DEC map nor in the anatomical slice, as shown in Figure 9. The projection of AND ROI are also represented with a semi-transparent green overlay. It was noticed that the high sensitivity regions shown in the sensitivity map corresponded to fiber tract branches located in the anterior and posterior sides of FAT, which were not part of the desired bundle. This state corresponds to Scenario 3.3, as discussed in Section 5. To achieve the complete and correct Scenario 1.3, the suggested course of action involves shrinking the seed ROI to the low homogeneous sensitivity region while considering the sensitivity map and ROI projection. The resulting ROI and the fiber tracts are shown in Figure 10b. The resulting fiber tracts are validated by our collaborators. With the utilization of the sensitivity map, the user achieved the desired fiber tracts in just one iteration, which would otherwise take four iterations of ROIs adjustments and manipulations in the automatic pipeline.

We had a general feedback session with our collaborators regarding the proposed visualization and guidance strategies. They agreed that our proposed visualization strategy could improve their understanding of the sensitivities in the ROIs and help in defining the accurate ROI for the bundle by using the provided visual guidance. Our collaborators were enticed by the interactive definition of the ROIs and especially by the projection visualization of the AND region. However, it was remarked that usability needs to be further studied, which we plan to do in future work.

8. Conclusion and Future work

There are several parameters in the fiber tracking pipeline that considerably affect the results. In this work, we have presented an approach to use seed-point sensitivity to guide ROI definition in the fiber tracking pipeline. We have analyzed the use of sensitivity for ROI definition and presented various scenarios that users experience in the ROI definition process. Based on the provided scenarios, corresponding guidance has been addressed. We have developed an interactive visualization approach as a proof of concept that allows users to investigate the region-based sensitivities and enables sensitivity-aware ROI definition by utilizing the computed seed-point sensitivity feature and projection map. Being able to visualize the sensitivity based on seed-point placement provides additional information to choose the optimal ROI. We also integrated our visualization framework with the automatic pipeline used by our collaborators. We explored the feasibility of using a sensitivity map to refine the automatically generated ROIs in a case where manual user input is required. The computed map provided guidance to the user in tuning the ROIs based on the sensitivity information and potentially saving various iterations for ROI adjustments.

While the utilization of color bins and transparency for the overlaid sensitivity map can help reduce clutter to some extent, the sensitivity map still overcrowds essential anatomical information, potentially impeding the user's ability to make accurate judgments. The enhancement of effectively integrating sensitivity information with anatomical data could be contemplated as a prospect for future research. For this study, we limit our work to isotropic pertur-

bation in the seed point. However, anisotropic variations in the seed point could also be explored. The selected distance measure used in sensitivity computation is capable of identifying bundle boundaries through proper bin selection. Nonetheless, there is room for exploring alternative measures to enhance the accuracy of bundle boundary detection even further.

We consider future work to develop a user study to evaluate our designed techniques and the effect of these sensitivities in the definition of ROIs. It would also be interesting to embed our work with other uncertainty visualizations [BWJ*03; SVBK14] of the DWI pipeline. This would facilitate gaining a better understanding of how uncertainties propagate through the whole system. Our clinical collaborators stress the relevance of adding uncertainty to their existing current workflow. However, the lack of access to tools that show uncertainty makes it difficult to evaluate its real benefit in practice. Our proposed solution is a step towards reducing this bottleneck.

9. Acknowledgments

This work is part of the research program "Diffusion MRI Tractography with Uncertainty Propagation for the Neurosurgical Workflow" with project number 16338, which is (partly) financed by the Netherlands Organisation for Scientific Research (NWO).

References

[AG95] ALT, HELMUT and GODAU, MICHAEL. "Computing the Fréchet distance between two polygonal curves". *International Journal of Computational Geometry & Applications* 5.01n02 (1995), 75–91 3.

[Bea02] BEAULIEU, CHRISTIAN. "The basis of anisotropic water diffusion in the nervous system–a technical review". *NMR in Biomedicine: An International Journal Devoted to the Development and Application of Magnetic Resonance In Vivo* 15.7-8 (2002), 435–455 1.

[BKP*04] BRUN, ANDERS, KNUTSSON, HANS, PARK, HAE-JEONG, et al. "Clustering fiber traces using normalized cuts". *Medical Image Computing and Computer-Assisted Intervention–MICCAI 2004: 7th International Conference, Saint-Malo, France, September 26-29, 2004. Proceedings, Part I 7*. Springer. 2004, 368–375 3.

[BML94] BASSER, PETER J, MATTIELLO, JAMES, and LEBIHAN, DENIS. "Estimation of the effective self-diffusion tensor from the NMR spin echo". *Journal of Magnetic Resonance, Series B* 103.3 (1994), 247–254 1.

[BPP*00] BASSER, PETER J, PAJEVIC, SINISA, PIERPAOLI, CARLO, et al. "In vivo fiber tractography using DT-MRI data". *Magnetic resonance in medicine* 44.4 (2000), 625–632 1, 4.

[BVPtH09] BRECHEISEN, RALPH, VILANOVA, ANNA, PLATEL, BRAM, and ter HAAR ROMENY, BART. "Parameter sensitivity visualization for DTI fiber tracking". *IEEE Transactions on Visualization and Computer Graphics* 15.6 (2009), 1441–1448 1, 2.

[BWJ*03] BEHRENS, TIMOTHY EJ, WOOLRICH, MARK W, JENKINSON, MARK, et al. "Characterization and propagation of uncertainty in diffusion-weighted MR imaging". *Magnetic Resonance in Medicine: An Official Journal of the International Society for Magnetic Resonance in Medicine* 50.5 (2003), 1077–1088 9.

[Cac81] CACUCI, DAN G. "Sensitivity theory for nonlinear systems. I. Nonlinear functional analysis approach". *Journal of Mathematical Physics* 22.12 (1981), 2794–2802 3.

[CFJ*05] COROUGE, ISABELLE, FLETCHER, P THOMAS, JOSHI, SARANG, et al. "Fiber tract-oriented statistics for quantitative diffusion tensor MRI analysis". *International Conference on Medical Image Computing and Computer-Assisted Intervention*. Springer. 2005, 131–139 3.

[CFJ*06] COROUGE, ISABELLE, FLETCHER, P THOMAS, JOSHI, SARANG, et al. "Fiber tract-oriented statistics for quantitative diffusion tensor MRI analysis". *Medical image analysis* 10.5 (2006), 786–798 3.

[CGG04] COROUGE, ISABELLE, GOUTTARD, SYLVAIN, and GERIG, GUIDO. "Towards a shape model of white matter fiber bundles using diffusion tensor MRI". *2004 2nd IEEE international symposium on biomedical imaging: nano to macro (IEEE Cat No. 04EX821)*. IEEE. 2004, 344–347 3.

[CMLZ08] CHEN, GUONING, MISCHAIKOW, KONSTANTIN, LARAMEE, ROBERT S, and ZHANG, EUGENE. "Efficient Morse decompositions of vector fields". *IEEE Transactions on Visualization and Computer Graphics* 14.4 (2008), 848–862 3.

[EYQ*20] ER, JIN, YUANJING, FENG, QINGRUN, ZENG, et al. "Data-driven automatic segmentation algorithm for trigeminal nerve fiber". *Chinese Journal of Biomedical Engineering* 39.4 (2020). Cited by: 0, 385–393 3.

[FBK*12] FEDOROV, ANDRIY, BEICHEL, REINHARD, KALPATHY-CRAMER, JAYASHREE, et al. "3D Slicer as an image computing platform for the Quantitative Imaging Network". *Magnetic resonance imaging* 30.9 (2012), 1323–1341 7.

[FTC*13] FARQUHARSON, SHAWNA, TOURNIER, J-DONALD, CALAMANTE, FERNANDO, et al. "White matter fiber tractography: why we need to move beyond DTI". *Journal of neurosurgery* 118.6 (2013), 1367–1377 1.

[GGTH07] GARTH, CHRISTOPH, GERHARDT, FLORIAN, TRICOCHE, XAVIER, and HANS, HAGEN. "Efficient computation and visualization of coherent structures in fluid flow applications". *IEEE Transactions on Visualization and Computer Graphics* 13.6 (2007), 1464–1471 3.

[Goo09] GOODLETT, CASEY BRETT. "Computation of statistics for populations of diffusion tensor images". PhD thesis. School of Computing, University of Utah, 2009 3.

[GSN*20] GUTIERREZ, CARLOS ENRIQUE, SKIBBE, HENRIK, NAKAE, KEN, et al. "Optimization and validation of diffusion MRI-based fiber tracking with neural tracer data as a reference". *Scientific reports* 10.1 (2020), 1–18 2.

[HB03] HARROWER, MARK and BREWER, CYNTHIA A. "ColorBrewer. org: an online tool for selecting colour schemes for maps". *The Cartographic Journal* 40.1 (2003), 27–37 6.

[HGT*10] HLAWITSCHKA, MARIO, GARTH, CHRISTOPH, TRICOCHE, XAVIER, et al. "Direct visualization of fiber information by coherence". *International journal of computer assisted radiology and surgery* 5 (2010), 125–131 3.

[HLZ*22] HUANG, JIAHAO, LI, MENGJUN, ZENG, QINGRUN, et al. "Automatic oculomotor nerve identification based on data-driven fiber clustering". *Human Brain Mapping* 43.7 (2022), 2164–2180 3.

[HSO*01] HOLODNY, ANDREI I, SCHWARTZ, THEODORE H, OLLENSCHLEGER, MARTIN, et al. "Tumor involvement of the corticospinal tract: diffusion magnetic resonance tractography with intraoperative correlation: Case illustration". *Journal of neurosurgery* 95.6 (2001), 1082–1082 1.

[HXA*18] HUO, YUANKAI, XU, ZHOUBING, ABOUD, KATHERINE, et al. "Spatially localized atlas network tiles enables 3D whole brain segmentation from limited data". *Medical Image Computing and Computer Assisted Intervention–MICCAI 2018: 21st International Conference, Granada, Spain, September 16-20, 2018, Proceedings, Part III 11*. Springer. 2018, 698–705 2.

[HZVM04] HUANG, HAO, ZHANG, JIANGYANG, VAN ZIJL, PETER CM, and MORI, SUSUMU. "Analysis of noise effects on DTI-based tractography using the brute-force and multi-ROI approach". *Magnetic Resonance in Medicine: An Official Journal of the International Society for Magnetic Resonance in Medicine* 52.3 (2004), 559–565 2.

[JC10] JONES, DEREK K and CERCIGNANI, MARA. "Twenty-five pitfalls in the analysis of diffusion MRI data". *NMR in Biomedicine* 23.7 (2010), 803–820 2.

[JD88] JAIN, ANIL K and DUBES, RICHARD C. *Algorithms for clustering data*. Prentice-Hall, Inc., 1988 4.

[JLT*13] JEURISSEN, BEN, LEEMANS, ALEXANDER, TOURNIER, JACQUES-DONALD, et al. "Investigating the prevalence of complex fiber configurations in white matter tissue with diffusion magnetic resonance imaging". *Human brain mapping* 34.11 (2013), 2747–2766 2.

[JMF99] JAIN, ANIL K, MURTY, M NARASIMHA, and FLYNN, PATRICK J. "Data clustering: a review". *ACM computing surveys (CSUR)* 31.3 (1999), 264–323 4.

[JPS*10] JIAO, FANGXIANG, PHILLIPS, JEFF M, STINSTRA, JEROEN, et al. "Metrics for uncertainty analysis and visualization of diffusion tensor images". *International Workshop on Medical Imaging and Virtual Reality*. Springer. 2010, 179–190 3.

[Laz10] LAZAR, MARIANA. "Mapping brain anatomical connectivity using white matter tractography". *NMR in Biomedicine* 23.7 (2010), 821–835 1.

[LMP*01] LE BIHAN, DENIS, MANGIN, JEAN-FRANÇOIS, POUPON, CYRIL, et al. "Diffusion tensor imaging: concepts and applications". *Journal of Magnetic Resonance Imaging: An Official Journal of the International Society for Magnetic Resonance in Medicine* 13.4 (2001), 534–546 2.

[LSM07] LEKIEN, FRANCOIS, SHADDEN, SHAWN C, and MARSDEN, JERROLD E. "Lagrangian coherent structures in n-dimensional systems". *Journal of Mathematical Physics* 48.6 (2007), 065404 3.

[MCCV99] MORI, SUSUMU, CRAIN, BARBARA J, CHACKO, VADAPPURAM P, and VAN ZIJL, PETER CM. "Three-dimensional tracking of axonal projections in the brain by magnetic resonance imaging". *Annals of Neurology: Official Journal of the American Neurological Association and the Child Neurology Society* 45.2 (1999), 265–269 1.

[MGB*18] MEUSCHKE, MONIQUE, GÜNTHER, TOBIAS, BERG, PHILIPP, et al. "Visual analysis of aneurysm data using statistical graphics". *IEEE transactions on visualization and computer graphics* 25.1 (2018), 997–1007 3.

[MV02] MORI, SUSUMU and VAN ZIJL, PETER CM. "Fiber tracking: principles and strategies–a technical review". *NMR in Biomedicine: An International Journal Devoted to the Development and Application of Magnetic Resonance In Vivo* 15.7-8 (2002), 468–480 2.

[MVB*16] MEUSCHKE, MONIQUE, VOSS, SAMUEL, BEUING, OLIVER, et al. "Combined visualization of vessel deformation and hemodynamics in cerebral aneurysms". *IEEE transactions on visualization and computer graphics* 23.1 (2016), 761–770 3.

[MVV05] MOBERTS, BART, VILANOVA, ANNA, and VAN WIJK, JARKE J. "Evaluation of fiber clustering methods for diffusion tensor imaging". *Proceedings of IEEE Visualization*. IEEE. 2005, 65–72 3, 4.

[NGH*05] NIMSKY, CHRISTOPHER, GANSLANDT, OLIVER, HASTREITER, PETER, et al. "Preoperative and intraoperative diffusion tensor imaging-based fiber tracking in glioma surgery". *Neurosurgery* 56.1 (2005), 130–138 1.

[OYA*22] ORTUG, ALPEN, YUZBASIOGLU, NESLIHAN, AKALAN, NEJAT, et al. "Preoperative and postoperative high angular resolution diffusion imaging tractography of cerebellar pathways in posterior fossa tumors". *Clinical Anatomy* 35.8 (2022), 1085–1099 1.

[PB96] PIERPAOLI, CARLO and BASSER, PETER J. "Toward a quantitative assessment of diffusion anisotropy". *Magnetic resonance in Medicine* 36.6 (1996), 893–906 1.

[PP99] PAJEVIC, SINISA and PIERPAOLI, CARLO. "Color schemes to represent the orientation of anisotropic tissues from diffusion tensor data: application to white matter fiber tract mapping in the human brain". *Magnetic Resonance in Medicine: An Official Journal of the International Society for Magnetic Resonance in Medicine* 42.3 (1999), 526–540 1.

[QRO*09] QAZI, ARISH A, RADMANESH, ALIREZA, O'DONNELL, LAUREN, et al. "Resolving crossings in the corticospinal tract by two-tensor streamline tractography: Method and clinical assessment using fMRI". *Neuroimage* 47 (2009), T98–T106 3.

[RW09] ROCKAFELLAR, R TYRRELL and WETS, ROGER J-B. *Variational analysis*. Vol. 317. Springer Science & Business Media, 2009 3.

[SBF*17] SCHLAIER, JUERGEN R, BEER, ANTON L, FALTERMEIER, RUPERT, et al. "Probabilistic vs. deterministic fiber tracking and the influence of different seed regions to delineate cerebellar-thalamic fibers in deep brain stimulation". *European Journal of Neuroscience* 45.12 (2017), 1623–1633 2.

[SHV21a] SIDDIQUI, FAIZAN, HÖLLT, THOMAS, and VILANOVA, ANNA. "A Progressive Approach for Uncertainty Visualization in Diffusion Tensor Imaging". *Computer Graphics Forum* 40.3 (2021), 411–422 1.

[SHV21b] SIDDIQUI, FAIZAN, HÖLLT, THOMAS, and VILANOVA, ANNA. "Uncertainty in the DTI Visualization Pipeline". *Anisotropy Across Fields and Scales*. Springer, Cham, 2021, 125–148 1.

[SKM*90] SEVICK, RJ, KUCHARCZYK, J, MINTOROVITCH, J, et al. "Diffusion-weighted MR imaging and T2-weighted MR imaging in acute cerebral ischaemia: comparison and correlation with histopathology". *Acta neurochirurgica. Supplementum* 51 (1990), 210–212 1.

[SP07] SADLO, FILIP and PEIKERT, RONALD. "Efficient visualization of Lagrangian coherent structures by filtered AMR ridge extraction". *IEEE Transactions on Visualization and Computer Graphics* 13.6 (2007), 1456–1463 3.

[SPH*06] SCHONBERG, TOM, PIANKA, PAZIT, HENDLER, TALMA, et al. "Characterization of displaced white matter by brain tumors using combined DTI and fMRI". *Neuroimage* 30.4 (2006), 1100–1111 3.

[SPW*07] SCHMAHMANN, JEREMY D, PANDYA, DEEPAK N, WANG, RUOPENG, et al. "Association fibre pathways of the brain: parallel observations from diffusion spectrum imaging and autoradiography". *Brain* 130.3 (2007), 630–653 2.

[SVBK14] SCHULTZ, THOMAS, VILANOVA, ANNA, BRECHEISEN, RALPH, and KINDLMANN, GORDON. "Fuzzy fibers: Uncertainty in dMRI tractography". *Scientific Visualization*. Springer, 2014, 79–92 1, 9.

[TCC07] TOURNIER, J-DONALD, CALAMANTE, FERNANDO, and CONNELLY, ALAN. "Robust determination of the fibre orientation distribution in diffusion MRI: non-negativity constrained super-resolved spherical deconvolution". *Neuroimage* 35.4 (2007), 1459–1472 2.

[TMA*09] TAOKA, TOSHIAKI, MORIKAWA, M, AKASHI, T, et al. "Fractional anisotropy–threshold dependence in tract-based diffusion tensor analysis: evaluation of the uncinate fasciculus in Alzheimer disease". *American Journal of Neuroradiology* 30.9 (2009), 1700–1703 1, 2.

[TRW*02] TUCH, DAVID S, REESE, TIMOTHY G, WIEGELL, METTE R, et al. "High angular resolution diffusion imaging reveals intravoxel white matter fiber heterogeneity". *Magnetic Resonance in Medicine: An Official Journal of the International Society for Magnetic Resonance in Medicine* 48.4 (2002), 577–582 2.

[VES16] VAN HECKE, WIM, EMSELL, LOUISE, and SUNAERT, STEFAN. *Diffusion tensor imaging: a practical handbook*. Springer, 2016 1.

[VW21] VOLTOLINE, RAPHAEL and WU, SHIN-TING. "Multimodal visualization of complementary color-coded FA map and tensor glyphs for interactive tractography ROI seeding". *Computers & Graphics* 96 (2021), 24–35. ISSN: 0097-8493 1–3.

[WH11] WEILER, FLORIAN and HAHN, HORST K. "An interactive ROI tool for DTI fiber tracking". *Medical Imaging 2011: Visualization, Image-Guided Procedures, and Modeling*. Vol. 7964. SPIE. 2011, 941–947 2, 3.

[ZDL03] ZHANG, SONG, DEMIRALP, CAGATAY, and LAIDLAW, DAVID H. "Visualizing diffusion tensor MR images using streamtubes and streamsurfaces". *IEEE Transactions on Visualization and Computer Graphics* 9.4 (2003), 454–462 3.